REKAYASAMESIN
eISSN 2477-6041 artikel 15, pp. 451 – 459, 2022
V13 N2

CORROSION BEHAVIOR OF LOW ALLOY Ni-Cr-Mo STEEL AFTER HOT FORGING FOLLOWED BY INTERCRITICAL HEATING FOR WEATHERED RESISTANT FASTENER

Miftakhur Rohmah
Junior Researcher
Research Center for Metallurgy,
National Research and Innovation Agency (BRIN)
Email: miftakhur.rohmah@brin.go.id / miftakhur.its@gmail.com

Gusti Galih Pandhita
Undergraduate Student
Materials and Metalurgy Engineering,
Institut Teknologi Kalimantan
Email: 06181032@student.itk.ac.id

Septian Adi Chandra
Junior Researcher
Research Center for Metallurgy,
National Research and Innovation Agency (BRIN)
Email: sept004@brin.go.id

Low Ni-Cr-Mo alloys is developed by thermomechanical process to obtain high strength, toughness, and great hardenability properties. the aim of this study is to determine the correlation between the microstructure and corrosion properties after hot forging and followed by intercritical heating with cooling rate variation. Low Ni-Cr-Mo steel was homogenized, hot forgings at 950℃, and heat treated at 880℃with three cooling variations by water, oil, and air. Intercritical heating makes a dual-phase structure. Metallorgaphy and hardness test is confirmed a mechanical properties. OCP and cyclic polarization test is confirmed a corrosion behavior. As the fast-cooling (water quenchant) show the lath martensite, bainite, and a few of acicular ferrite. The hardness of the 75-ton result is slightly lower than the 50-ton load, is reached 591±9.4 VHN for 75-ton and 597±15.6 VHN for 50-ton. Polarization test resulted corrosion resistance sample with 100 ton forging water quench has a high corrosion rate 0.8 mpy, higher than air quench 0.01 mpy.

Keywords: *Cyclic Polarization, Hot Forging, Intercritical Heating Low Ni-Cr-Mo alloy.*

1. INTRODUCTION

Over the past decades, continuous improvement has been made to acquaint High Strength Fastener Steel with increased strength and corrosion resistance. The produce of high-strength fastener steel that is appropriate for a high salt environment is a new challenge. AISI 8740 is a series nickel-chromium-molybdenum low alloy steel with high strength, good toughness, and great hardenability properties, which is not found in lower grade carbon steel. The forged Ni-Cr-Mo alloys are among the most versatile. This gradediscovers wide application in the automotive industry,particularly in ring gears, racks and helical gears, pins, bearing races, etc [1] [2]. In several amounts, chromium provides compact Cr_2O_3 protection in oxidizing conditions (nitric acid or sulfuric acid solution). Simultaneously, Mo energizes the resistance in a less oxidizing (dilute acid solution) and upgrades the localized corrosion resistance [3] [4].

Numerous studies have developed corrosion resistance, mainly from microstructural modification by working on the thermomechanical and heat treatment process. The hot forged steel with low 1% Cr-0.20% Mo consists of superfine acicular bainitic ferrite and refined martensite phase, leading to higher combinations of yield stress and total elongation. The microstructure of the hot-forged steel is often governed by the size and type of matrix structure, earlier austenitic grain size, second phase properties, and retained austenite characteristics [5]. Regrettably, low Ni-Cr-Mo steel shows low hot plasticity, making it difficult to deform at high temperatures [6]. In addition, the dual-phaseprovides a compressive long-range internal stress in soft pro-eutectoid ferrite. Dislocation density was founded to expand the austenite phase during hot forging. Besides that, carbide precipitation (Cr_2N, M_7C_3, or $M_{23}C_6$) and sensitization arenot expected in Ni-Cr-Mo alloys due to the negative effect on the corrosion resistance and plasticity [5] [6]. So, controlling the parameter of hot forging, especially in the heating and cooling stage, is imperative to acquire low Ni-Cr-Mo alloy without phase precipitation.

Low alloy steel's mechanical and corrosion resistance depends on its composition, thermo-mechanical history, and resulting microstructure. Martensite is the main factor in deciding the high

Corresponding Author: miftakhur.rohmah@brin.go.id Received on: October 2021 Accepted on: March 2022
DOI: https://doi.org/10.21776/jrm.v13i2.1055

mechanical and corrosion of the fastener. High strength is commonly provided by normalized and tempered, oil-or water quenched and tempered conditions or the annealed condition due to having formed martensite [7]. Herbirowo et al. [8] found that heat treatment of Ni-Cr-Mo Modification steel by oil quench and quench temper has resulted in moderate hardness (around 43.6 HRc) dan high wear resistance (about 0.1 g/cm^2) due to martensite formed. Nakhaie et al. [9] also detailed that grain boundaries, twin boundaries, and martensitic phase boundaries with stress concentration are all subject to preferential corrosion due to their high chemical activity. The hot-forged preform distributes residual stress and has excellent machinability and a surface that can be changed by chemical or mechanical treatment. However, there is limited research investigating the effect of intercritical heating on microstructure and corrosion properties in the hot-forged low alloy Ni-Cr-Mo steel. To obtain low Ni-Cr-Mo alloy with optimal mechanical properties and corrosion resistance, it is necessary to know the optimal load forged and cooling rate of hot forging deformation.

2. METHOD AND MATERIALS

2.1. Materials

The steel used in this experiment is low Ni-Cr-Mo alloys, which are prepared by investment casting. The nickel laterite, ferrochrome, ferromanganese, and ferromolybdenum are alloyed in the induction furnace Inductotherm butterfly type at 1550-1650 ℃. After homogenization, the chemical composition of molten metal of Ni-Cr-Mo is determined by Optical Emission Spectroscopy (OES) Bruker Q4 Tasman, asshown in Table 1. The design of these steels is comparable to AISI 8740. The Ni-Cr-Mo casting alloy is milled, which is then used as a forging sample.

Table 1. Chemical composition of low Ni-Cr-Mo alloys

Materials	C	Cr	Ni	Mo	Mn	Si	S	P
Ni-Cr-Mo Alloys	0.4438	0.598	0.4273	0.3234	0.853	0.3988	0.0003	0.0121
AISI 8740	0.38-0.43	0.4-0.6	0.4-0.7	0.2-0.3	0.75-1	0.15-0.3	0.04	0.035

2.2. Hot Forging and Intercritical Heating Process

Six samples with a dimension of Ø20 cm and 20 cm in height are subjected tothe hot forging process. The surface is flattened with SiC paper to reduce a forging defect. All samples were heated at austenitization temperature of 950℃ for 1 hour in a muffle furnace (heating rate 5℃/s). Hot-forged in open die-one stage up to a reduction strain of 18-30% using a 50 and 75-ton hot-forging machine followed by intercritical heating at 880 for 1 hour. Intercritical heating makes a dual-phase structure. To obtain high mechanical and corrosion properties, the different cooling rate is used: water, oil, and open-air cooling.

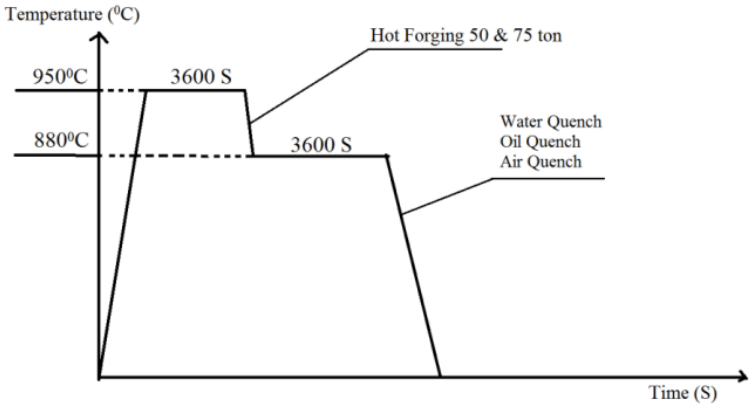

Figure 1. The schematic of the thermomechanical process of low Ni-Cr-Mo alloys

2.3. Metallographic and Hardness Test

For a metallographic test, all samples were prepared in 1x1 cm form, mounted with epoxy resin. Thus, the pieces were wet-grounded with SiC paper (up to 2000 grit) and polished with 1 µm alumina paste to attain a

mirror-like surface. Therefore, the specimens are rinsed in an ultrasonic cleaner with deionized water. Metallographic testing was carried out using an Olympus BX-53M optical microscope and 2% Nital etch. At the same time, the five indentations of hardness test were carried out by Micro-Vickers tester with 5N loaded for 10 s.

2.4. Polarization Test

The polarization test specimens were cut 1x1 cm, soldered with copper wire for electrical contact, and mounted with epoxy resin. Hence, all samples were wet grounded up to 800 grit and polished by 1 µm alumina to reduce a scratch and assure the fresh film formation.The polarization test was carried out using the Cyclic Polarization method in Gamry G-750 Instruments Potentiostats to study corrosion at a surface. Cyclic polarization is described in ASTM G61. The potentiostats record the applied current to the cell that gives the increase in potential. Three electrodes as reference electrode (saturated calomel electrode), as a counter electrode (platinum wire), and as working electrode (the sample), which all of them was connected in a circuit cell. All the tests are performed in 3.5 %wt--NaCl solution at room temperature. Before the polarization test, specimens are immersed in the solution for 3600s for open-circuit potential (E_{ocp}) measurement. For pitting observation, the voltage is swept across a -0.5 V until 1.5 V range (5 mV/s of forwarding scan), but then reversed back to the starting potential, with a 2.5 mV/s reverse scan.

3. RESULT AND DISCUSSION

3.1 Continuous Cooling Transformation (CCT) Diagram of Low Ni-Cr-Mo Alloys

CCT Diagram was simulated using JMatPro version 12, which predicts an austenite transformation with a different cooling rate. CCT Diagram depends on temperature and holding time of austenitization stage, which is depicted in Figure 2. The parameter in the CCT Diagram construction is 950℃ austenitization, grain size 14.5 µm and chemical composition that has been shown in Table 1.

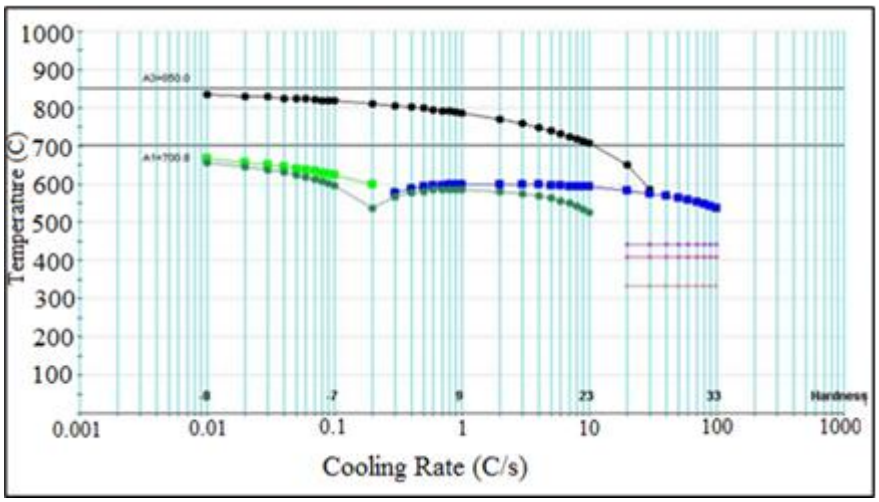

Figure 2. CCT Diagram of AISI 8740 (black = ferrite, light green = pearlite, dark green = retained austenite, blue = bainite, and violet = martensite)

Based on Figure 2, the full bainite transformation didn't occur in 0.3-100 ℃/s cooling rate but will frame along with other phases such as pro-eutectoid ferrite (0.01 – 12 ℃/s), retained austenite (0.01-10 ℃/s), and lath martensite (11-100 ℃/s). Other than that, the low Ni-Cr-Mo alloy might contain bainite-ferrite in the lower cooling rate (0.3-10 ℃/s) and bainite-martensite in the fast cooling (12-100 ℃/s) – the increasing cooling rate leading to the decrease of bainite start (Bs) temperature. Transformation into bainite at the cooling rate of 0.3 ℃/s was around 587℃. Martensite start temperature at the cooling rate 20℃/s was around 441℃. It shows a very similar result to the CCT diagram of SA508 Gr4N reported by Kim [10] and 2¼ Cr-1Mo steel written by Tartaglia [11]. The higher cooling rate can drive force for the transformation, which suppresses the pro-eutectoid ferrite formation, increasing the nucleation sites of bainite. In addition, the hot deformation can cause dislocation and provide more nucleation [12].

3.2 Microstructure analysis

The effect of forging loaded and cooling rate on the microstructure of low Ni-Cr-Mo steel is depicted in Figure 3 with a magnification of 500x. The microstructure is dependent on the steel composition and thermomechanical history.

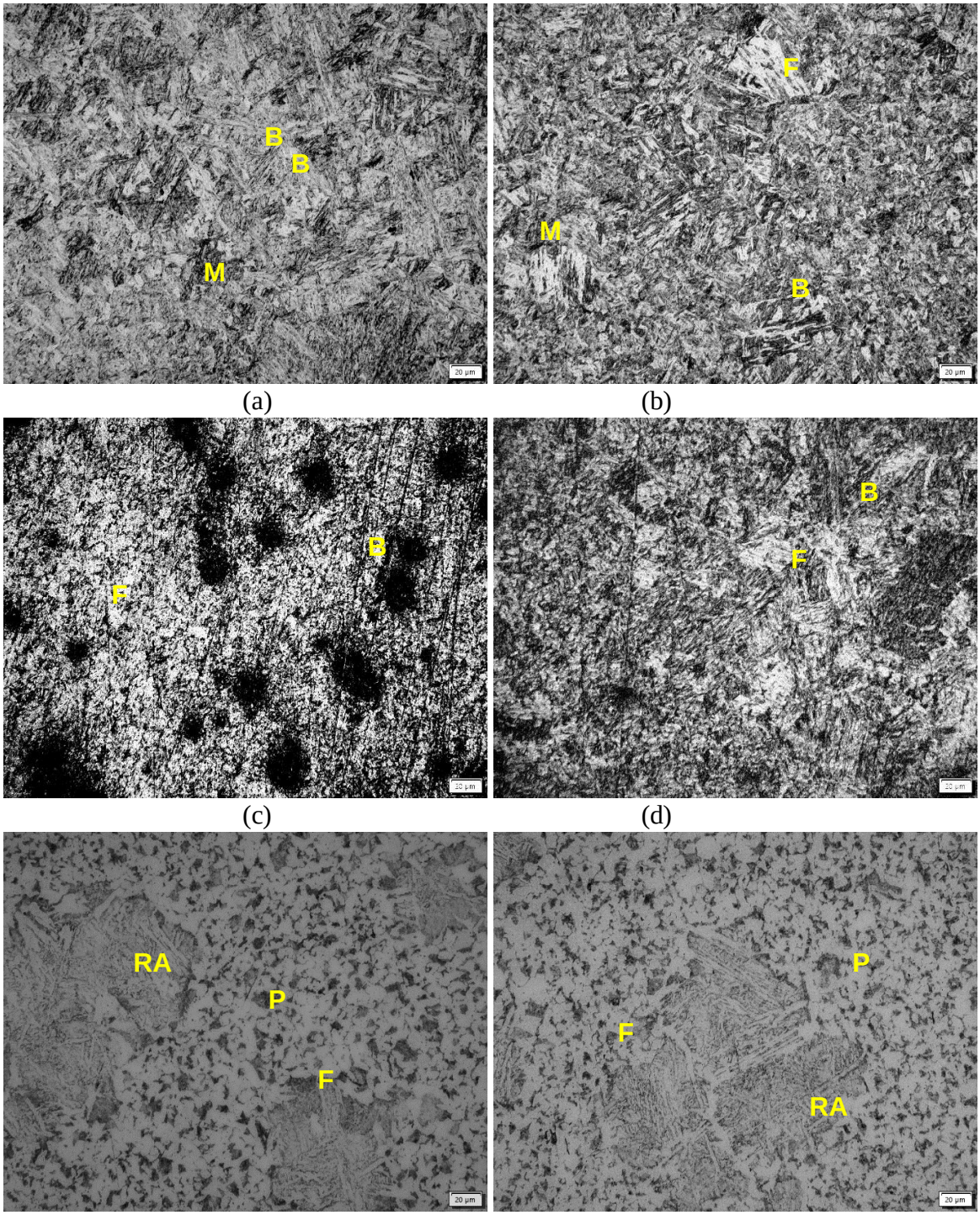

Figure 3. Microstructure of low Ni-Cr-Mo after hot forging (a) 50-ton, (b) 75-ton water quench, (c) 50-ton, (d) 75-ton oil quench, (e) 50-ton, (f) 75-ton air cooling.

From Figure 3, the final microstructure of Low Ni-Cr-Mo alloy is dominated by bainite structure. At low temperatures, the microstructure of Ni-Cr-Mo steel is regularly in the ferrite combination, while at high temperatures, the microstructure is in the austenite phase. As the fast-cooling (water quenchant) result, Fig 3 (a,b) show the lath martensite (likely needle form),bainite, and a few of acicular ferrite (slightly pointed

shape) were consistently distributed. Acicular ferrite is caused by ferrite growth without diffusion, becomes saturated in carbon in 0.01-12℃/s of cooling rate. Martensite is caused by carbon caught in body-centered tetragonal structure with the diffusion-less shear process. The metastable phase depends on the non-equilibrium cooling, the chemical composition, and section size of the forging [13]. Martensite lath has gradually been refined with the cooling rate increase [14]. In the moderate cooling rate (oil quenchant), Fig 3(c,d) comprise of acicular bainite and ferrite. Fig 3(e,f) shows the pearlite and ferrite phase in the slow cooling rate. The relatively fine grain structure and substructure of martensite and bainite allow superior strength and toughness properties compared to ferritic-pearlitic [13].

All microstructure has related to CCT Diagram in Figure 2. The chromium and carbon addition had a decreasing the bainite start-finish and martensite start-finish. Cr is carbide forming element, which can delay the pearlite transformation. Mo can decrease the ferrite transformation temperature but increase the diffusion activation energy of carbon in austenite and reduce the diffusion coefficient of carbon. It can also effectively promote the formation of acicular ferrite [14].

For understanding the forged load effect, Fig 3(a,c,e) is compared to Fig 3(b,d,f). It clearly shows that the 75-ton load has a slight refine than the 50-ton result. The differences may have resulted from pressure deformation percentage during hot forging. On the other hand, as a result of the hot forging, a refined grain structure is produced and provides segregation breaking up, void closure, grain size reduction, and fibrous grain flow [13].

3.3 Hardness analysis

In this work, the microhardness test confirmed the resistance of localized plastic deformation induced by mechanical indentation. The precisely cut diamond are used for the test with lighter loads. The hardness value of low Ni-Cr-Mo after hot forging is depicted in Figure 4.

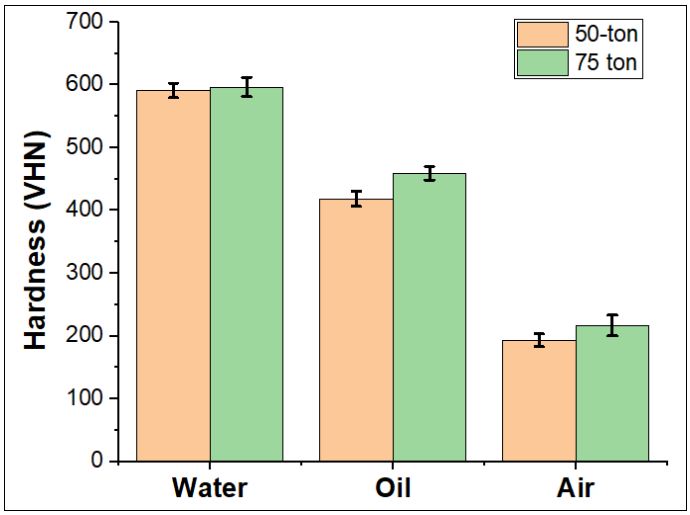

Figure 4. Hardness of Ni-Cr-Mo after forging followed by intercritical heating

According to Fig 4, the hardness of the 75-ton result is slightly lower than the 50-ton load. In addition, the hardness increased with the increase of the cooling rate. In fast cooling with water quenchant, the highest hardness is reached 591±9.4 VHN for 75-ton and 597±15.6 VHN for 50-ton. Itis indicated that the grain size becomes refined elongated, and the high density of defect during thermomechanical caused by the increasing reduction ratio, which gives rise to strengthening mechanism and severely affects the phase transformation [15]. However, hot deformation provides the driving force for microstructure transformation that depends on recrystallization and grain growth during heat treatment addition. During the quenching, a thermal cycle occurred which is affect the thermal gradient, thermal flux, and cooling rate. The water cooling has a lower temperature faster than oil, and tends to increase in hardness as result of the martensite formation [16].

3.4 Polarization Analysis

The open-circuit potential is the potential where the total anodic current equals the total cathodic current. In cyclic polarization, the voltage is swept across a range but then reversed to the starting potential. The surface

is likely to be changed by the reactions during the scan. The corrosion behavior is influenced by microstructure, grain size, alloy composition, secondary phase, oxide/passive film formed, residual stress, and corrosion environment [17]. The OCP is shown in Figure 5 and Table 2.

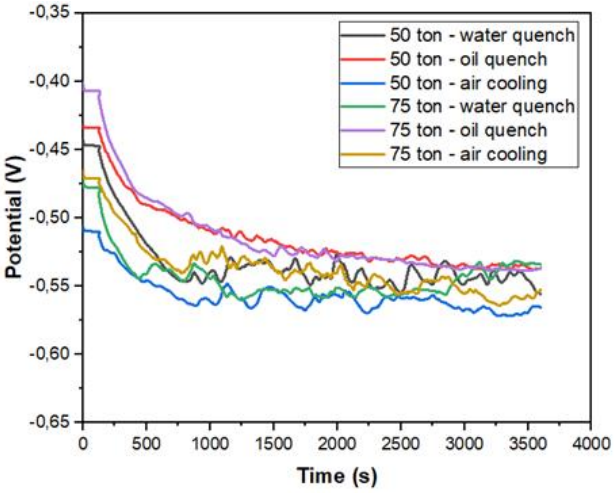

Figure 5. OCP curve of low Ni-Cr-Mo steel in 3.5% NaCl solution

Table 2. OCP parameter of low Ni-Cr-Mo Alloy

Sample		**Open Circuit Potential (V vs SCE)**
50-ton	Water quench	-0.556 to -0.443
	Oil quench	-0.538 to-0.432
	Air cooling	-0.572 to -0.506
75-ton	Water quench	-0.542 to-0.459
	Oil quench	-0.539 to -0.401
	Air cooling	-0.560 to -0.471

From Fig 5 and Table 2, initial OCP values of all samples are ranged from -400 mV to – 500 mV. In general, the potential corrosion declines quickly or moves toward electronegative at 500 s, but the steady stable-constant value of E_{OCP} is invisible after immersion 3600 s. A smaller the Eoc value is indicates the specimen has low corrosion resistance [18]. The specimen after water cooling has low Eoc (-0.572 V for 50-ton and -0.560 V for 75-ton). The decreasing OCP can be attributed to the strong removal of the natural oxide layer "semi-stable" on the Ni-Cr-Mo surface. At lower potentials, Ni-Cr-Mo is shown to initiate pitting corrosion, and the presence of chloride ions can also strengthen the passive layer shown by OCP oscillations towards electropositive values. Chloride ions present aggressively attack the iron surface leading to a continuous dissolution of iron. The film formed is very dynamic, forming and dissolving as Ni-Cr-Mo interact with the NaCl environment [19]. Several corrosion products as $FeCl_2$, $Fe(OH)_2$, and $Fe(OH)_3$ may form during pitting corrosion [20]. Fe, Cr, Co, Ni, and Mo tends to passive layer in angstroms thickness. The iron chloride formation accelerates the dissolution by attacking its surface and leading to the shape of the pits on its surface, as can be explained by following reaction (1)-(7) [21].

$$Fe + Cl^- \rightarrow Fe(Cl^-)_{surface} \quad (1)$$

$$Fe(OH)_{surface} + Fe(Cl^-)_{surface} \rightarrow Fe + FeOH^+ + Cl^- + 2e^- \quad (2)$$

$$FeOH^+ + H^+ \rightarrow Fe^{2+}{}_{solution} + H_2O \quad (3)$$

$$Fe_{surface} + 2Cl^- \rightarrow FeCl_{2\ surface} + 2e^- \quad (4)$$

$$FeCl_{2\ surface} + Cl^-_{(aq)} \rightarrow FeCl_{3\ surface} + e^- \quad (5)$$

$$FeCl_{3\ surface} = FeCl_{3\ interface} \rightarrow FeCl_{3\ solution} \quad (6)$$

The different cooling rate in intercritical heating leads to microstructure evolution and have an impact in corrosion behavior. OCP curve with 75-ton load is more positive (+5 mV) than 50-ton load. Other than, the oil quench of both load forged is more positive than water and air cooling. Multiphase in Ni-Cr-Mo can induce micro-galvanic reaction and negatively lead to corrosion resistance.

A cyclic polarization was performed for confirmation of anodic-cathodic behavior in low Ni-Cr-Mo steel. This curve is shown in Figure 6, which indicates pitting corrosion without a re-passivation mechanism. The low current density (I_{corr}) and high corrosion potential (E_{corr}) indicate good corrosion resistance.

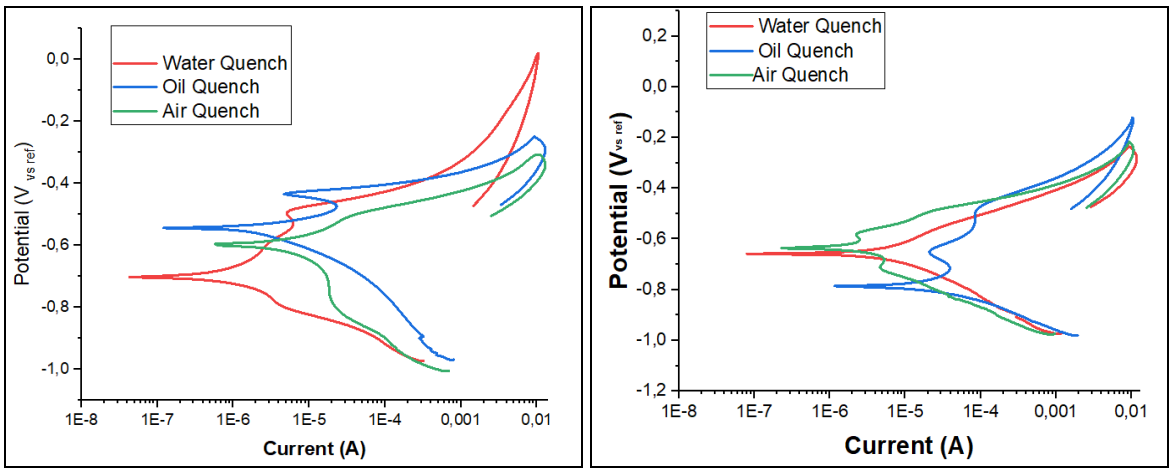

(a) (b)

Figure 6. Cyclic polarization of low alloy Ni-Cr-Mo steel after (a) 50-ton (b) 75-ton forged load

From Fig 6, all samples exhibit active dissolution behavior (or no passivation) without completing a positive hysteresis loop due to 50 and 75-ton followed by heat treatment. It's indicated that the corrosion process is still active and tend to metastable pit for all samples. Self-passivity process had not occurred in the present work due to the lower chromium content of 0.8-9% [22]. Positive hysteresis is related to the decrease of the passivity due to localized corrosion (pitting and crevice corrosion) [23]. The anodic and cathodic polarization obviously changes for each sample, show the different mechanisms for corrosion reaction. At the beginning of the measurement, a cathodic current is related to the reduction of oxygen. The lower cooling rate shift the cathodic curve to upper right, while the anodic curve moves downwards. It is shown that the heat treatment provides a more positive corrosion potential, and the corrosion current density is getting smaller, which means the corrosion rate is getting smaller.

The water-quench had the polarization curve at the far left and bottom for the 50-ton load forged according to Fig 6(a). With the slow cooling rate, i.e., air-quench, the curve shifts upward but slightly to the right, indicating the potensial corrosion (Ecorr) is more positive and the current is more larger (Fig 6a). The oil-quenched sample had the highest corrosion rate, is around ~0.687 mpy, and the air-quenched sample had the lower corrosion rate (around 0.474 mpy). At the same water cooling condition, the curve polarization of 50-ton has a more negative Ecorr (around -707.8 mV) and a smaller Icorr (around to 1.183 µA) if compared to a 75-tons sample (Fig 6b). The martensite and bainite cause a higher corrosion rate, so the electrochemical activity increases with martensite content up to 6% and further decreases pitting resistance. It is noted that the martensite phase is less noble compared to the bainite phase due to micro-galvanic corrosion between M/A island and bainite ferrite [24][25]. But this tendency didn't happen for water and air quenched. The 50-ton sample had a more positive Ecorr (approximately to -544.4 mV) in oil quench, but the Icorr is more smaller (~ 1.505 µA) than 75-tons. Without martensite phase in coupled, the finer bainite and ferrite had good effect on the corrosion rate, is decrease up to 0.064 mpy. In air cooled, the 50-ton sample had a more positive Ecorr (~595.2 mV) and a larger Icorr (1.038 µA). In general, the both sample with air cooling condition had the smallest corrosion rate that is due to the contribute of pearlite and ferrite phase. The ferrite phase is preferentially corroded from inside the boundary and pearlite acts as cathodic [26].

The electrochemical parameter of all samples was obtained by using Tafel fitting, as listed in Table 3. The decreased cooling rate and increased load forged reduce the critical pitting potential, namely -6.146 mV, -252.1 mV, and -303.2 mV for water, oil, and air cooling. In addition, with oil quenching, there is an unstable transition behavior around -434.75 mV for 50-ton and -645.8 mV for 75-ton, like the anodic "nose" observed

on polarization curves of active-passive metals. There are attributed to the nucleation, growth, and passivation of metastable on the surface and correlated with the different phases due to low Cr, Fe, Ni [27].

Table 3. Corrosion properties of low Ni-Cr-Mo steel

Sample	Uniform Corrosion				Pitting Corrosion	
	Beta (V/dec)	Ecorr (mV)	Icorr ($x10^{-6}$ A)	Corrosion rate (mpy)	Potential (mV)	Potential ($x10^{-3}$ A)
50 ton – water	285.2 x 10^{-3}	-707.8	1.183	0.54	-6.146	10.20
50 ton – oil	40.87x 10^{-3}	-544.4	1.505	0.687	-252.1	9.627
50 ton – air	58.64x 10^{-3}	-595.2	1.038	0.474	-303.2	10.10
100 ton – water	104.2x 10^{-3}	-648.6	1.770	0.8089	-236.7	9.948
100 ton – oil	110.6x 10^{-3}	-785.7	0.140	0.064	-161.3	10.06
100 ton – air	51.95x 10^{-3}	-631.6	0.0367	0.017	-219.7	9.710

4. CONCLUSION

Low Ni-Cr-Mo steel has been successfully developed through the hot forging followed by the intercritical heating process. The load forged, cooling rate, and chemical composition gives significant effect on the microstructure, hardness, and corrosion properties. The microstructure obtained is consist of ferrite, pearlite, martensite, bainite, and retained austenite in 50&75-ton. In addition, the grain size of the 50-ton forging loading tends to be larger with flat shaped when compared to the 75-ton loads caused by rapid growth in the intercritial heating process. Thus, the hardness value of the sample with a load of 75-tons is harder. In the corrosion properties, the lower cooling rate shift the cathodic curve to upper right, while the anodic curve moves downwards. The heat treatment provides a more positive corrosion potential, and the corrosion current density is getting smaller, and the corrosion rate is getting smaller. Sample with 100 tons load water quench has the maximum corrosion rate 0.8089 mpy, and sample with 100 tons load air quench (normalizing) has the minimum corrosion rate 0.017 mpy.

5. ACKNOWLEDGEMENT

The authors would like to thanks all of the research group member “Rekayasa Paduan Logam dan Manufaktur” who have contributed to the technical and design of experiment. This research is fully funded by DIPA 2019 Program in the Research Center for Metallurgy and Materials, Indonesian Institute of Sciences.

6. REFERENCE

[1] ARULMANI, L., SHRIDHARMURTHY, H. N., SELVAN, M.C.P., and MADARA, S.R., “Hot powder forging behavior analysis of sintered AISI 8740 PM steels for automotive application,” *Mater. Today Proc.*, v. 28, n. 2, February, pp. 1068–1072, 2019, doi: 10.1016/j.matpr.2020.01.079.

[2] ALVES, H., and HEUBNER, U., *Aqueous Corrosion of Nickel and its Alloys*, 1st ed., Amsterdam: Elsevier Ltd., 2016.

[3] HOU, Y., LI, Y., ONODERA, E., ZHANG, C., KOIZUMI, Y., and CHIBA, A., “Ex-situ observation on the dissolution behaviour of Ni-16Cr-15Mo and Ni-30Co-16Cr-15Mo alloys in hydrofluoric acid,” *Corros. Sci.*, v. 90, pp. 133–139, 2015, doi: 10.1016/j.corsci.2014.10.003.

[4] YANG, B., LI, J., GONG, X., NIE, Y., and LI, Y., “Effects of Cu addition on the corrosion behavior of NiCoCrMo alloys in neutral chloride solution,” *RSC Adv.*, v. 7, n. 65, pp. 40779–40790, 2017, doi: 10.1039/c7ra05617f.

[5] SUGIMOTO, K.I., SATO, S. H., KOBAYASHI, J., and SRIVASTAVA, A.K., “Effects of Cr and Mo on mechanical properties of hot-forged medium carbon TRIP-aided bainitic ferrite steels,” *Metals (Basel).*, v. 9, n. 10, p. 1066, 2019, doi: 10.3390/met9101066.

[6] ANGELESCU, M.L., COJOCARU, V.D., ŞERBAN, N., and COJOCARU, E.M., “Evaluation of optimal forging temperature range for an industrial UNS S32750 SDSS alloy using SEM-EBSD analysis,” *Metals (Basel).*, v. 8, n. 7, 2018, doi: 10.3390/met8070496.

[7] M. F. ASHBY AND D. R. H. JONES, “Steels 2—Alloy Steels,” In: *Eng. Mater. 2*, pp. 221–236, 2013, doi: 10.1016/b978-0-08-096668-7.00013-9.

[8] HERBIROWO, S., SYAHRUM, M., HASBI, M.Y., CHANDRA, S.A., RIDLO, F.M., and

ADJIANTORO, B., "Mechanical and microstructure properties of the Ni-Cr-Mo modified steel by heat treatment process," *IOP Conf. Ser. Mater. Sci. Eng.*, vol. 541, no. 1, p. 012014, 2019, doi: 10.1088/1757-899X/541/1/012014.

[9] NAKHAIE, D., and MOAYED, M.H., "Pitting corrosion of cold rolled solution treated 17-4 PH stainless steel," *Corros. Sci.*, v. 80, pp. 290–298, 2014, doi: 10.1016/j.corsci.2013.11.039.

[10] HONG, S., *et al.*, "Effect of cooling rate on mechanical properties of SA508 Gr.1A steels for main steam line piping in nuclear power plants," *Int. J. Press. Vessel. Pip.*, v. 191, February, p. 104359, 2021, doi: 10.1016/j.ijpvp.2021.104359.

[11] TARTAGLIA, J.M., KUELZ, A.N. and THELANDER, V.H., "The Effects of Alloying Elements on the Continuous Cooling Transformation Behavior of 2¼Cr-1Mo Steels," *J. Mater. Eng. Perform.*, v. 27, no. 12, pp. 6349–6364, 2018, doi: 10.1007/s11665-018-3683-1.

[12] ZHOU, X., CHEN, Y., JIANG, Y., and LI, Y., "Effects of plastic deformation on austenite transformation in Fe-1.93Mn-0.07Ni-1.96Cr-0.35Mo ultra-high strength steel during continuous cooling," *Mater. Res. Express*, v. 6, no. 12, pp. 0–9, 2019, doi: 10.1088/2053-1591/ab6e7c.

[13] GARZA, E.I.S., "*Mechanical Properties and Microstructure of Large Steel Forgings for Applications in the Energy Sector*,", Thesis, The University of Sheffield, 2017.

[14] YANG, X., *et al.*, "Effect of Cooling Rate and Austenite Deformation on Hardness and Microstructure of 960MPa High Strength Steel," *Sci. Eng. Compos. Mater.*, v. 27, pp. 415–423, 2020, doi: 10.1515/secm-2020-0045.

[15] TASH, M.M., ALKAHTANI, S.A., and ABUHASEL, K.A., "Effect of Hot Work on Hardness and Impact Toughness of Heat Treated Low Alloy Steels," *Adv. Mater. Res.*, v. 1082, February 2016, pp. 197–201, 2014, doi: 10.4028/www.scientific.net/amr.1082.197.

[16] BUDIANTO, E., CHOIRON, M.A., and DARMADI, D.B., "Hardening Baja AISI 1045 Menggunakan Gel Aloe Vera Sebagai Media Pendingin," *J. Rekayasa Mesin*, v. 7, n. 2, pp. 55–64, 2016, doi: 10.21776/ub.jrm.2016.007.02.3.

[17] CHU, Y., CHEN, Y., CHEN, Y., LIU, P., and LI, X., "Microstructure and Corrosion Behavior of Ni-Cr-Mo Nickel-based Alloy Weld," *Mater. Res.*, v. 23, n. 6, pp. 1–9, 2020, doi: 10.1590/1980-5373-MR-2019-0631.

[18] ANGGRIAWAN, O., CHOIRON, M.A., and LIN, J., "Pengaruh Waktu Pemanasan (Anil) Terhadap Ketahanan Korosi Pada Gelas Metalik Berbasis Zirkonium," *Rekayasa Mesin*, v. 5, n. 3, pp. 193–199, 2014.

[19] LI, X., and OGLE, K., "The Passivation of Ni-Cr-Mo Alloys: Time Resolved Enrichment and Dissolution of Cr and Mo during Passive-Active Cycles," *J. Electrochem. Soc.*, v. 166, n. 11, pp. C3179–C3185, 2019, doi: 10.1149/2.0201911jes.

[20] ANSARI, T.Q., LUO, J.L., and SHI, S.Q., "Modeling the effect of insoluble corrosion products on pitting corrosion kinetics of metals," *npj Mater. Degrad.*, v. 3, pp. 1–12, 2019, doi: 10.1038/s41529-019-0090-5.

[21] SHERIF, E.S.M., "A comparative study on the electrochemical corrosion behavior of iron and X-65 steel in 4.0 wt % sodium chloride solution after different exposure intervals," *Molecules*, v. 19, n. 7, pp. 9962–9974, 2014, doi: 10.3390/molecules19079962.

[22] QIAN, Y.H., NIU, D., XU, J.J. and LI, M.S., "The influence of chromium content on the electrochemical behavior of weathering steels," *Corros. Sci.*, v. 71, pp. 72–77, 2013, doi: 10.1016/j.corsci.2013.03.002.

[23] ESMAILZADEH, S., ALIOFKHAZRAEI, M., and SARLAK, H., "Interpretation of Cyclic Potentiodynamic Polarization Test Results for Study of Corrosion Behavior of Metals: A Review," *Prot. Met. Phys. Chem. Surfaces*, vol. 54, pp. 976–989, 2018, doi: 10.1134/S207020511805026X.

[24] BÖSING, I., BOBROV, I., EPP, J., BAUNE, M., and THÖMING, J., "Influence of systematically changed martensite content on the passive film properties of austenitic stainless steel in neutral electrolyte," *Int. J. Electrochem. Sci.*, v. 15, pp. 319–333, 2020, doi: 10.20964/2020.01.09.

[25] WEI, J., DONG, J. H., KE, W., and HE, X.Y., "Influence of inclusions on early corrosion development of ultra-low carbon bainitic steel in NaCl solution," *Corrosion*, v. 71, n. 12, pp. 1467–1480, 2015, doi: 10.5006/1837.

[26] NEETU, KATIYAR, P.K., SANGAL, S., and MONDAL, K., "Effect of various phase fraction of bainite, intercritical ferrite, retained austenite and pearlite on the corrosion behavior of multiphase steels," *Corros. Sci.*, vol. 178, p. 109043, 2021, doi: 10.1016/j.corsci.2020.109043.

[27] SHI, Y., *et al.*, "Homogenization of AlxCoCrFeNi high-entropy alloys with improved corrosion resistance," *Corros. Sci.*, vol. 133, pp. 120–131, 2018, doi: 10.1016/j.corsci.2018.01.030.